Effect of Mg and La substitution on Electromagnetic Properties of Ni-Cu-Zn Ferrite

A THESIS SUBMITTED IN PARTIAL FULFILLMENT OF
THE REQUIREMENTS FOR THE DEGREE OF
BACHELOR OF TECHNOLOGY

By
PRAKASH PRADHAN
Roll No.-108CR013

DEPARTMENT OF CERAMIC ENGINEERING
NATIONAL INSTITUTE OF TECHNOLOGY
ROURKELA
20011-2012

Effect of Mg and La substitution on Electromagnetic Properties of Ni-Cu-Zn Ferrite

A THESIS SUBMITTED IN PARTIAL FULFILLMENT OF
THE REQUIREMENTS FOR THE DEGREE OF
BACHELOR OF TECHNOLOGY

By
PRAKASH PRADHAN
Roll No.-108CR013

UNDER THE GUIDANCE OF
DR. JAPES BERA

DEPARTMENT OF CERAMIC ENGINEERING
NATIONAL INSTITUTE OF TECHNOLOGY
ROURKELA
20011-2012

CERTIFICATE

NATIONAL INSTITUTE OF TECHNOLOGY
2012

This is to certify that the thesis entitled, **"Effect of Mg and La Substitution on Electromagnetic Properties of Ni-Cu-Zn Ferrite"** submitted by **Prakash Pradhan** in partial fulfillment of the requirements of the award of Bachelor of Technology Degree in Ceramic Engineering at the National Institute of Technology, Rourkela is an authentic work carried out by him under my supervision and guidance.

To the best of my knowledge, the matter embodied in the thesis has not been submitted to any other university / institute for the award of any Degree or Diploma.

Date:

Dr. Japes Bera
(Head of the Department)
Dept. of Ceramic Engineering
National Institute of Technology
Rourkela-769008

ACKNOWLEDGEMENT

With deep regards and profound respect, I take this opportunity to express my deep sense of gratitude and indebtedness to Prof. Japes Bera, Head of the Department, Department of Ceramic Engineering, N. I. T. Rourkela, for introducing the research topic and for his inspiring guidance, constructive criticism and valuable suggestion throughout this research work. It would have not been possible for me to bring out this project report without his constant help and encouragement. I wish that he will keep in touch with me in future and will continue to give his valuable advice.

I am also grateful to all the faculties of Department of Ceramic Engineering, whose vast knowledge in the field of Ceramics has enlightened me in different areas of this research work.

I am also thankful to Mr. Sanjaya Kumar Swain, Mr. Ganesh Kumar Sahoo, Miss Geetanjali Parida and other research scholars in Department of Ceramic Engineering for their help and support.

Submitting this report would not be possible without the help, support and suggestions from my friends. I am very much thankful to them.

Finally, I thank my parents for their support and encouragement.

Date:

PRAKASH PRADHAN
ROLL NO: 108CR013
B.Tech, Ceramic Engineering
NIT ROURKELA

ABSTRACT

NiCuZn ferrite is a very important material for multilayer chip inductor core material. La & Mg substituted NiCuZn ferrites have been reported in different literature for their improved electromagnetic properties. However there is no report of simultaneous substitution La and Mg in NiCu Zn ferrite. The present project focuses on the effect of simultaneous substitution of Mg and La in NiCuZn ferrite. All the compositions were synthesized through auto-combustion method. The nano-crystalline ferrite powders were successfully synthesized by this method. The powders were characterized for their phase formation using XRD. After calcination at 700^0C the powders were pressed in to pellet and toroid specimens. The specimens were sintered at different temperatures and characterized for their bulk density, microstructural development, dielectric and ferromagnetic properties. Initial permeability of all the ferrites was measured on toroid specimen using LCR meter. Magnetization behavior was investigated in a magnetometer. On an average the electromagnetic properties of La doped NiCuZn ferrite enhanced compare to Mg – substituted ferrite.

List of Figures

List of Tables

CONTENTS

CHAPTER I

INTRODUCTION

Introduction:

Ferrites are usually used as a core material in inductor. An Inductor is an impedance device which has a coil with or without core for introducing inductance to an electronic circuit. The ferrite core typically multiplies the inductance of a coil by the permeability of the core. Generally the core is in the shape of a rod or toroid. Ferrite should have not only high magnetic permeability but also have good DC characteristics i.e. as small decrease in magnetic permeability with DC.

Now days it is very important to reduce the size and weight of various type of electronic apparatus. For that, there is a high demand of reduction in size with high performance for electronic components. To meet this demand inductors are fabricated in a multilayer structure containing ferrite and electrode layers in a single body. Generally silver 'Ag' conductors are used as a coil in multilayer. So ferrite materials need to be sintered at a lower temperature than the melting point of silver (about 900^0C). To achieve this requirement copper is introduced in NiZn ferrite to form Ni-Cu-Zn ferrite with an effective sintering temperature below 900^0C. Many Patented composition of Ni-Cu-Zn ferrites are available in literature. For example, US patent no. 2011/0226982 A1 [1] and many others.

Ni-Cu-Zn ferrite has been the dominant material for multilayer chip inductor magnetic core application because they have good electromagnetic properties [2-3]. They have also good temperature dependency of initial permeability which is very low or limited.

NiCuZn ferrite has the spinel structure. Spinel has the general formula MFe_2O_4, where M is divalent metal ion. The spinel lattice is consists of an oxygen closed-packed arrangement in which 32 oxygen ions form a unit cell. Two kinds of interstices in between the closed-packed anions as shown in Fig.1: a) tetrahedrally coordinated interstices (called 'A' site) and b)

octahedrally coordinated interstices (called ‘B’ site). Structurally spinel can be represented as AB_2O_4. One unit cell of it contains eight formula units of AB_2O_4, where, out of 64 ‘A’ sites 8 and out of 32 ‘B’ sites 16 are occupied by cations.

Depending on the cation distribution in interstices, the spinel is broadly divided into two groups: a) normal spinel and b) inverse spinel. NiCuZn ferrite is a solid solution of inverse $NiFe_2O_4$, $CuFe_2O_4$ and normal $ZnFe_2O_4$ ferrites. Due to the favorable fit of charge distribution, Ni^{2+} and Cu^{2+} ions show strong preference to ‘B’ sites. Zn^{2+} ions show a strong preference for ‘A’ sites due to its electronic configuration. The structural formula can be represented by:

$$(Zn_yFe_{1-y})[Ni_{1-x-y}Cu_xFe_{1+y}]O_4 \qquad (1.1)$$

where, first bracket is represented by tetrahedral ‘A’ site and third bracket is represented by octahedral ‘B’ site.

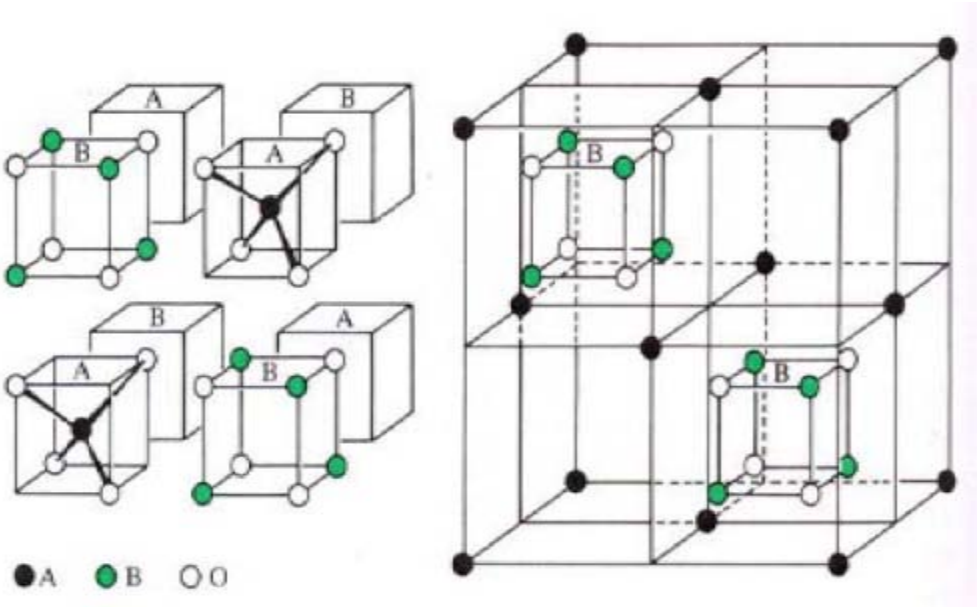

Fig.1 Two sub cells of a unit cell of the spinel structure

The magnetic properties of the ferrites are dependent on the distribution of cations in 'A' and 'B' sites through substitution. Typical example is the substitution of Ni by Zn. NiCu ferrite is inverse spinel where, half of the Fe^{3+} are in 'A' sites; remaining half and Ni, Cu share 'B' sites. When Zn is substituted for Ni, Zn preferentially enters into the 'A' sites by displacing a proportionate number of Fe^{3+} from 'A' to 'B' sites with a cation distribution as stated in equation (1.1). The net effect is the significant increase in magnetic moments in octahedral site as well as in the unit cell.

The major parameters used for evaluating magnetic materials are Permeability and resistivity. The electromagnetic properties of NiCuZn ferrites are highly sensitive to the processing parameters especially sintering conditions and the amount of constituent metal oxides in their composition [4-5].

Various compositions in the system $(Ni_{1-x-y}Zn_xCu_y)Fe_2O_4$ has been investigated. To decrease the sintering temperature so that it can be co-fired with Ag internal electrode Cu is introduced in the structure. But, Cu decreases the resistivity of the ferrite, which is not desirable for its high frequency applications. That is why, optimization of Cu content with respect to densification and resistivity of the ferrite is required. Different ranges of electromagnetic properties have been reported with various Zn concentrations in NiCuZn ferrites. Similarly, optimization of Zn concentration is essential to achieve desirable electromagnetic properties in the ferrites where, Zn enters into the 'A' sites (Fig 1.1) by displacing a proportionate number of Fe^{3+} from 'A' to 'B' sites.

Permeability in spinel ferrite can be increased by lowering the magnetostriction constant. It has been seen that magnetostriction constant of MgCuZn ferrite is lower than NiCuZn ferrite, so it is expected to increase the permeability Mg can be substituted for Ni in the ferrite where, Mg

enters into the ‘B’ sites (Fig 1.1) and displaces a proportionate number of Ni^{2+}. Mg containing compositions were also preferred to avoid the presence of divalent iron (to obtain high resistivity) and to avoid the tendency of discontinuous grain growth.

Influence of rare earths on the properties of different ferrites has been reported by many investigators. Rare earth ions can improve densification and increase permeability and resistivity in $(Ni_{1-x-y}Zn_xCu_y)RE_zFe_{2-z}O_4$ ferrites where, RE enters into the ‘B’ sites (Fig 1.1) by displacing a proportionate number of Fe3+ from ‘B’ to ‘A’ sites. V_2O_3, MoO_3 and Bi_2O_3 were reported to be the most widely used sintering additives for the ferrites. Further research is needed on the mixed sintering additives in the system V_2O_5, Bi_2O_3 and MoO_3 for the ferrites.

Several studies have been conducted to enhance the properties of NiCuZn ferrite. Important approaches adopted are: (a) the reduction of the particle size to improve densification, (b) using sintering aids for better densification and (c) substitutions at tetrahedral and octahedral crystallographic site in the spinel ferrite to improve electromagnetic properties.

1.1 Objective of the Present Work:

Various works has been carried out with substitution of Mg or La in the NiCuZn spinel structure separately. This has shown significant improvements in the electromagnetic properties of NiCuZn ferrite. With this background the present Objective of the work is to synthesize nano crystalline NiCuZn ferrite with simultaneous substitution of Magnesium and Lanthanum through citrate-nitrate sol-gel auto-combustion synthesis process and to investigate the effect of Magnesium and Lanthanum on various electromagnetic properties of NiCuZn ferrite

CHAPTER II

LITERATURE REVIEW

Introduction:

In this chapter, an attempt has been made to provide detailed review of the works carried out by various researchers on the synthesis of the NiCuZn ferrite, effect of divalent cation substitution as well as the effect of rare earth element substitution in these ferrites.

To improve the electro-magnetic properties various works has been carried out by many researchers. One of such attempt is to substitute divalent cations (M^{2+}); Ni, Cu, Zn, Mg, Co or mixture of these metal ions.

Chuangui Jin et. al. [6] investigated the structural and magnetic properties of $Ni_{0.4-x}Zn_{0.6}Cu_xFe_2O_4$ (x=0–0.2) synthesized by the co-precipitation method having with$NaOH$andNa_2CO_3 as co-precipitators. Specimens with NaOH co-precipitator showed lower saturation magnetization than the specimen with Na_2CO_3 as co-precipitator. Grain growth was found to be hindered for the specimen with Na_2CO_3 as co-precipitator this can be attributed to the existence of carbonates in the precursor powders.

Jin Woo Hahn et. al.[7] studied the boron substituted NiZnCu ferrite prepared through conventional ceramic method. They found an increase in density, shrinkage and saturation magnetization with increasing sintering temperature. An appropriate additive of boron was capable of enhancing densification; improve quality factor, magnetic moment of NiZnCu ferrite. NiZnCu ferrites with 0.2 mol% boron exhibited high quality factor and can be considered a promising material for multilayer chip inductors

P. Guzdek et. al. [8] prepared ferrite samples$Ni_{0.3}Zn_{0.62}Cu_{0.08}Fe_2O_4$ by the solid-state reaction method. Formation of cubic spinel structure was detected by X-ray diffraction patterns. They found that dielectric constant decreases with increase in frequency, and shows dielectric dispersion at lower frequencies. Saturation magnetization value of 82 emu/g and small coercivity

(0.5 kOe) was obtained for a ferrite composition of $Ni_{0.3}Zn_{0.62}Cu_{0.08}Fe_2O_4$. The same ferrite composition has high dc resistivity and highest inductance (300nH) therefore no isolator between the coil and the magnetic material is required. Mechanical, thermal, electrical and magnetic properties make the above ferrite the most suitable material for LTCC multi-layer substrates and microwave applications.

Yulan Jing et. al.[9] studied the effect of Mg-substitution on electromagnetic properties of low temperature fired NiCuZn ferrite synthesized by conventional mixed oxide method. They found that initial permeability increases with increase in Mg substitutions. However properties such as sintering density and magnetic flux density, remanence magnetization decreases with increase in Mg substitution due to that atomic weight of Mg is lower than Ni and due to the decrease of net magnetic moment respectively. Also, coercivity, and Snoek's product decrease with increase in Mg substitutions.

K.H.Rao et. al.[10] investigated the structural and magnetic properties of Mg substituted NiCuZn ferrites synthesized by sol-gel method and stated that the lattice constant reduces with increasing Mg content. Room temperature saturation Magnetization and coercivity showed reverse trend with increasing Mg content. Curie temperature (Tc) obtained from the thermo magnetic curves increases with Mg concentration. The initial permeability decreases with increasing Mg content, due to reduction in magnetisation, grain size and increase in magneto crystalline anisotropy constant.

P.K.Roy et.al.[11] worked on the Mg substitution on $(Ni_{0.25-x}Mg_xCu_{0.2}Zn_{0.55})Fe_2O_4$ with x =0.0, 0.07, 0.13, 0.18, and 0.25 and reported that the crystallite size of the ferrite powders synthesized

by the nitrate-citrate auto combustion method were about 19-22 nm and The permeability and AC resistivity were found to increase and the magnetic loss decreased with Mg substitution for Ni, up to x=0.18. The very high permeability in the composition x=0.18, was due to better densification, lower magnetostriction constant and inner stresses etc. The AC resistivity of the composition was also highest.

The rare earth substituted different ferrites are becoming the promising materials for different applications. Addition of small amount of rare earth ions to ferrite samples produces a change in their magnetic and electrical as well as structural properties depending upon the type and the amount of rare earth elements used.

P.K. Roy et. al.[12] investigated the effect of Lanthanum ion substitution for iron in $(Ni_{0.25}Cu_{0.20}Zn_{0.55})La_xFe_{2-x}O_4$ with x=0.0,0.0025, 0.050 and 0.075. They found that density, crystallite size, grain size, residual macrostress and initial permeability were affected by the Lanthanum substitution. Permeability and AC resistivity were found to increase and magnetic loss decreased with La substitution for Fe, upto x=0.025.Saturation magnetization and coercive field also increases upto that limit. The electromagnetic properties were found best in the ferrite composition of x=0.025.

CHAPTER III

EXPERIMENTAL PROCEDURE

3.1 Synthesis of Ferrite Powders

For the synthesis of ferrite powders Sol-Gel Auto-combustion route was followed. The raw materials used for this were as follows: Nickel Nitrate [$Ni(NO_3)_2.6H_2O$], Magnesium Nitrate [$Mg(NO_3)_2.6H_2O$], Zinc Nitrate [$Zn(NO_3)_2.6H_2O$], Copper Nitrate [$Cu(NO_3)_2.3H_2O$], Iron Nitrate [$Fe(NO_3)_3.9H_2O$], Lanthanum Oxide [La_2O_3], Citric Acid [$C_6H_8O_7.H_2O$]. All the chemicals were of standard grade and purity.

Sol-Gel Auto-combustion Synthesis

Substituted NiCuZn Ferrites i.e. Mg substituted, La substituted, both Mg & La substituted ferrites were prepared by the sol-gel auto-combustion synthesis. This method has various advantages over other method of synthesis. Such as inexpensive precursors, low external energy consumption, a simple preparation method as well as simple equipment requirement that result into nano-sized, homogeneous, highly reactive powders [13]. Auto combustion synthesis, also called self-propagating synthesis, was initially developed in Russia by Merzhanov and had been successfully used to speed up the synthesis of complex oxide material such as ferrites and high temperature superconductors [14].

Combustion synthesis proceeds through a highly exothermic redox reaction between metal nitrates and an organic fuel. Here the energy needed for the reaction between the component oxides is provided by the auto-combustion reaction itself and we don't need any external source of energy. Metal nitrates and organic fuel are mixed in water to form an aqueous solution. After that this solution is heated to transform it in to gel. By this molecular level of mixing between the precursor elements is achieved.

After the ignition starts, the dried gel burns in a self-propagating manner till all the gel burnt out. The reaction is self-propagating and is able to sustain this from 1 to 5 seconds typically, to form the desired product. This technique produces a homogenous product in a short amount of time without the use of expensive high temperature furnaces.

Various controlling parameters such as the type of fuel, the fuel-to-oxidizer ratio (f/o), the water content of the precursor mixture and the ignition temperature greatly affects the synthesis process. The fuel to oxidizer ratio also plays a critical role in influencing the reaction. A way to control the flame temperature of the reaction is by varying the amount of fuel to oxidizer.

The elemental stoichiometric coefficient, φe, is used to control the ratio of fuel to oxidizer in the reaction and is expressed as [15]:

$$\varphi_e = \frac{\sum \text{Total valencies of oxidizing elements in the nitrates and fuel}}{(1)\sum \text{Total valencies of reducing elements in the nitrates and fuel}} \qquad (3.1)$$

φe represents the ratio between the oxidizing and reducing components of the metalnitrate/ fuel mixture. When φe = 1, the reaction is stoichiometric. When φe < 1, the metal-nitrate/fuel mixture is fuel rich where as if φe > 1, the mixture is fuel lean and the mixture does not have enough fuel for the reaction to go to completion.

The flow diagram for the auto-combustion synthesis has been shown in fig. 2. Ferrite powders were synthesized by an amount of 10 gm per batch. The no of moles of various precursor materials required for synthesizing 10 gm of ferrite are given in the Table 1:

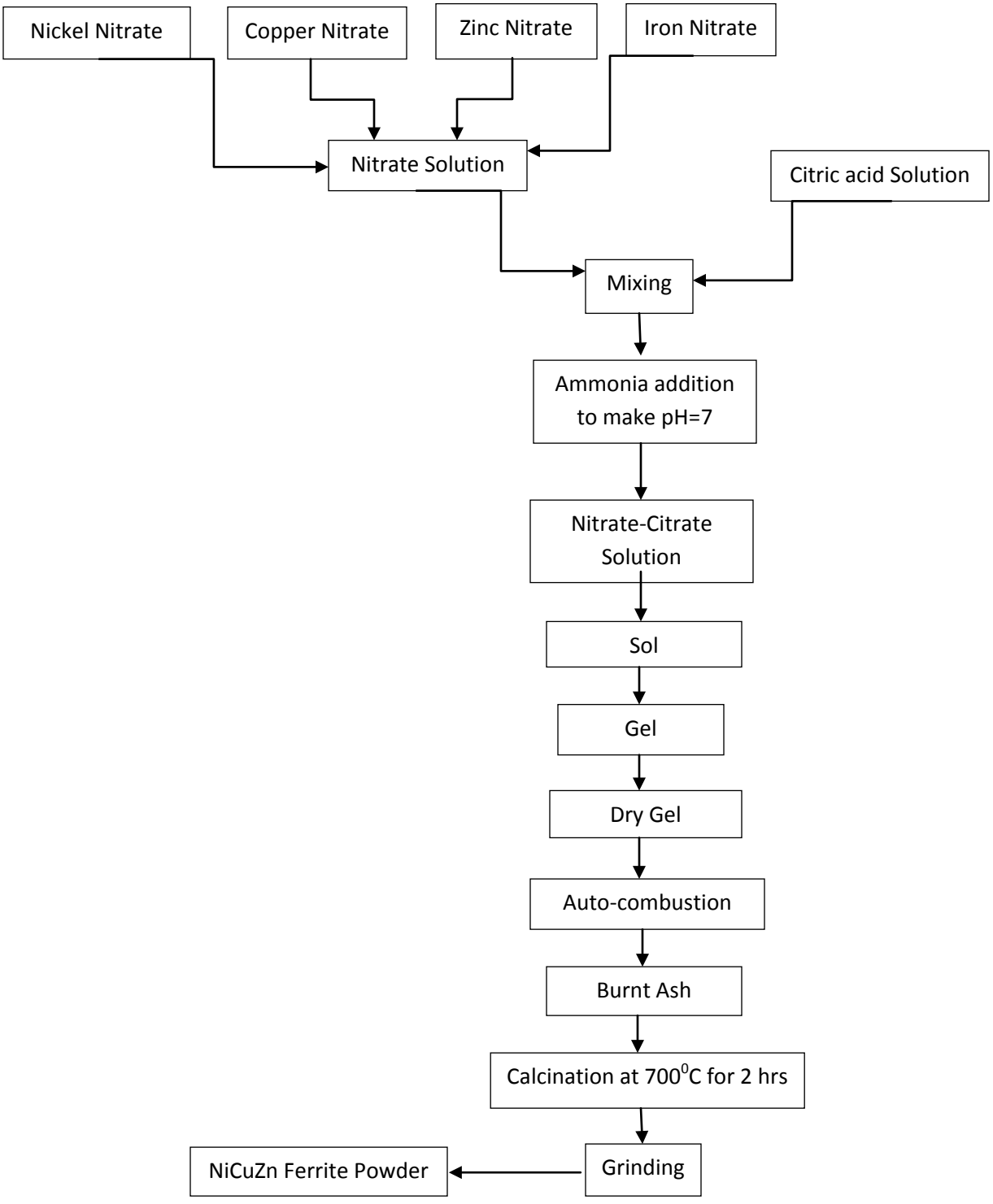

Fig. 2 Flow Diagram of Synthesis of NiCuZn ferrite through Sol-Gel Auto-combustion synthesis

Now required amounts of nitrates were added to form a 0.5 M solution and then 0.5 M separately prepared citric acid solution was added to it. The beaker containing the solution was placed over a magnetic stirrer and continuous stirring was done to get a completely homogeneous mixture. After that the solution was made to a pH=7 by the addition of ammonia solution. Then heating was started at 80^0C. With continuous stirring and heating the sol gradually transformed into a gel.

Here for the synthesis of La substituted and Mg & La substituted ferrite powders we had used Lanthanum oxide in place of Lanthanum nitrate. So in order to get Lanthanum nitrate in the solution we had to add nitric acid before the addition of citric acid solution which generally reacts with Lanthanum oxide in the following manner:

$$La_2O_3 + 6HNO_3 \longrightarrow 2La(NO_3)_3 + 3H_2O \qquad (3.2)$$

Once the dried gel was obtained the magnetic stirrer was removed from the beaker and the heating was increased to 200^0C. Upon ignition, dried gel burnt in a self-propagating combustion manner until all gels were completely burnt out to form a fluffy loose structure as shown in Fig.3. The fluffy material was ground to get ferrite powder. The as-burnt ash was calcined at 700°C for 2 hrs to get better crystallization and homogeneous cation distribution in the spinel and finally ground to get NiCuZn ferrite powders.

Table 1 No. of moles of various precursor materials required for synthesizing 10 gm of ferrite

	Ni-nitrate	Cu-nitrate	Zn-nitrate	Mg-nitrate	Fe-nitrate	Lanthanum oxide	Total
Mg- ferrite	0.0031	0.0086	0.0236	0.0077	0.086	---	0.13
La- ferrite	0.011	0.0082	0.0228	---	0.0816	0.0005	0.124
Mg&La ferrite	0.0029	0.0084	0.0232	0.0076	0.0836	0.00053	0.126

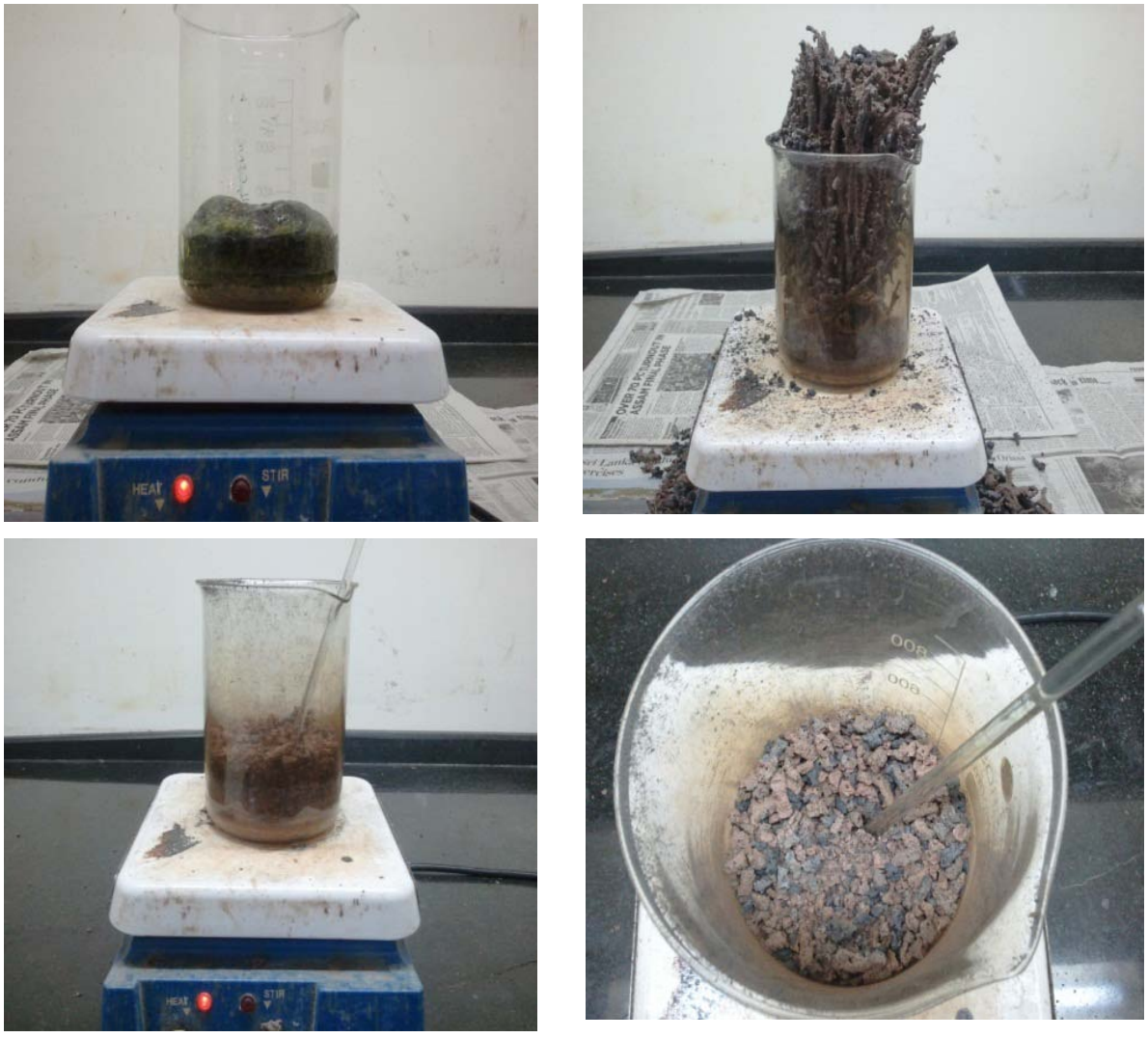

Fig. 3 Photographs of various stages of Auto-combustion synthesis process

3.2 Powder characterization

Phase Analysis

Phase formation of as burnt and calcined ferrite powder samples were studied by the powder X-ray diffraction performed with a Philip's Diffractometer (model: PW-1830, Philips, Netherlands). To detect the diffracted X-rays, an electronic detector is placed on the other side of the sample from the X-ray tube, and rotated the sample through different Bragg's angles. The goniometer keeps track of the angle (θ), and the detector records the detected X-rays in units of counts/sec and sends this information to the computer. After scan of the sample, the X-ray intensity (counts/sec) was plotted against the angle theta (2θ). The angle (2θ) for each diffraction peak was then converted to *d*-spacing, using the Bragg's law; $n\lambda = 2d \sin\theta$,

where λ is the wave length of x-ray and n is order of diffraction.

The identification of different phases was carried out by using Philips X-pert high score software.

3.3 Fabrication and Sintering of Ferrite Samples

The calcined powder of each batch was thoroughly mixed with 3 wt% binder (Polyvinyl alcohol) and was processed as per the flow chart (Fig 4).

The calcined powders were taken and PVA binder was added and mixed for 1 hrs. The mixed powder was dried and granulated. The granules were uniaxially pressed using a hydraulic press at a load of 3TON for 2 minutes to form pellets (Do-15 mm, thickness-2 mm) and toroid (Do-15 mm, Din-6 mm, thickness 2 mm). Green densities were calculated from weight/volume ratio.

Weight was measured using electronic balance whereas volume was calculated from the dimension of the specimens.

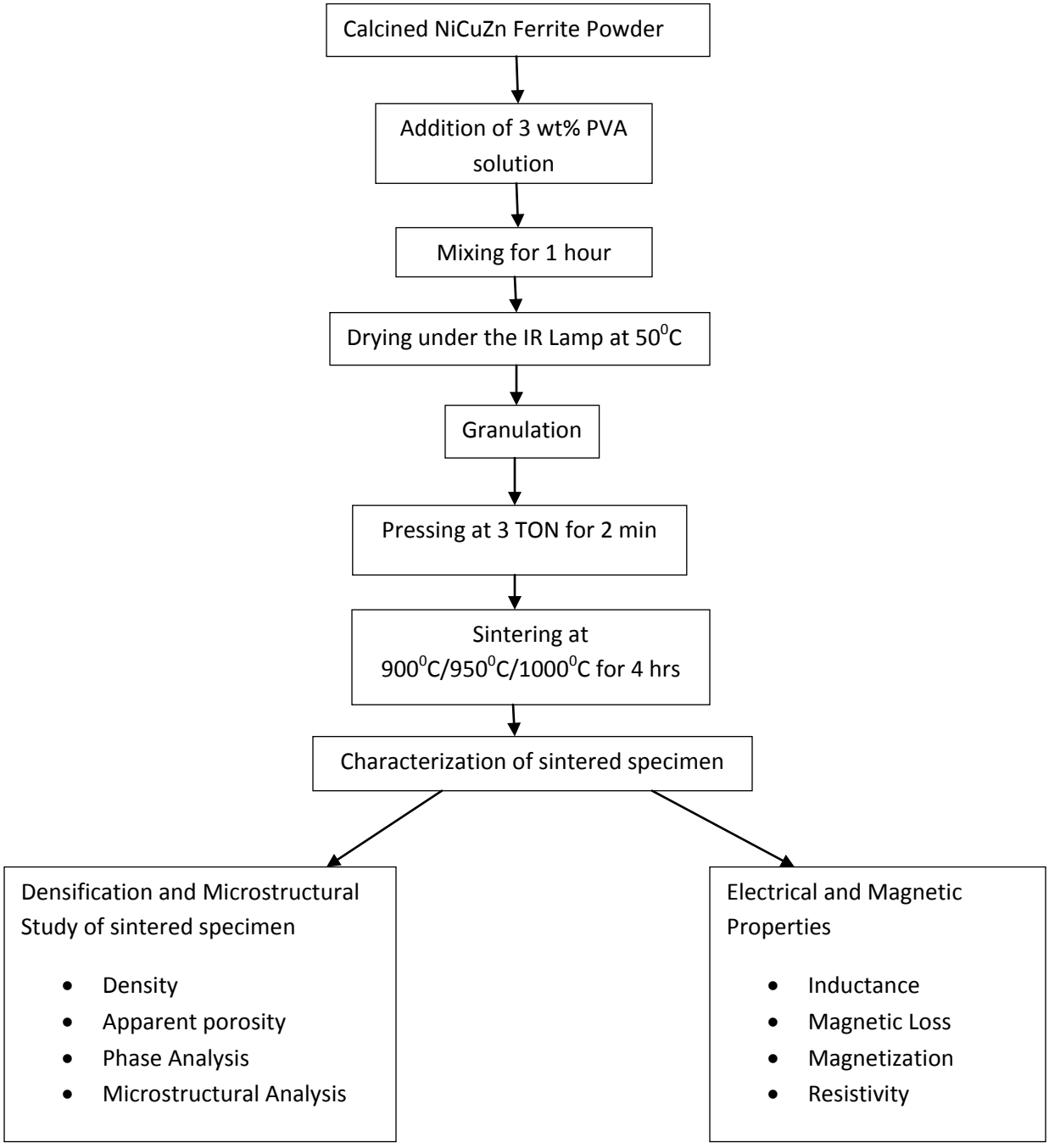

Fig. 4 Flow Diagram of Fabrication of ferrite samples and characterizations performed

3.4 Characterization of sintered specimen

Various physical properties such as apparent porosity, bulk density, phase analysis and microstructural analysis were carried out. Finally the electrical and magnetic properties were also measured for the sintered samples.

3.4.1 Apparent Porosity and Bulk Density

Apparent porosity and Bulk density of sinter specimens were determined by Archimedes principle. Dry weights of the sintered samples were noted down. Then the samples were immersed in water in a beaker and kept on a heater/ hot plate for 3 hrs for boiling so as to ensure that water filled up the open pores completely. Then, soaked and suspended weights were measured. The apparent porosity and bulk density were calculated as follows: Dry weight of the sample = D, Soaked weight of the sample = So , Suspended weight of the sample = Su

$$\text{Apparent Porosity} = \frac{So - D}{So - Su} \times 100 \qquad (3.3)$$

$$\text{Bulk Density} = \frac{D}{So - Su} \qquad (3.4)$$

The XRD density also calculated from XRD analysis and by comparing it with the dimensional density the relative density was also measured. XRD density is very important to measure as it gives more accurate result than the dimensional density which is generally associated with errors due to the presence of pores and cracks in the samples. This XRD density is sometimes also called the “Theoretical Density” although it is calculated from the experimental data.

The XRD density is given by the ratio of no. of atoms per unit cell to the volume of the unit cell.

i.e $$b = \frac{\sum A_w}{NV} \quad (3.5)$$

where, $\sum A_w$ = sum of atomic weights of all the atoms present in the unit cell

N = Avogadro's number

V = Volume of the unit cell

As the NiCuZn ferrite is of the spinel structure it contains 8 formula units in one unit cell. So we can write

$$b = \frac{8M_w}{Na^3} \quad (3.6)$$

where, M_w = Molecular weight

a = lattice parameter

N = Avogadro's Number

Now the % apparent porosity can be calculated by the following formula,

$$\%\text{Porosity} = \frac{XRD\ density - Bulk\ density}{XRD\ density} \times 100 \quad (3.7)$$

3.4.2 Microstructural Analysis

Microstructures of the sintered samples were studied by Scanning Electron Microscopy (SEM) analysis. Here in SEM an electron gun under vacuum emits a beam of electrons which is allowed to pass through a series of electromagnetic lenses before being allowed to fall on the specimen surface. The acceleration voltage of the electron beam is in the range of 1-30kv. Due to the interaction of the electron beam with the sample surface a part of the beam is reflected as back

scattered electron (BSE) beam along with low energy secondary electron (SE) beam, cathode luminescence, X-ray excitation beam and some part of the electron beam is transmitted.

Images formed from the (SE) beam were studied in the extrinsic mode of SEM. The emitted secondary electrons are detected and displayed on a scanning TV display. A bright image will be the result of high secondary electron emission, while the primary influence on high emission is the surface structure of the specimen. The end result is therefore brightness associated with surface characteristics and an image which looks very much like a normally illuminated subject.

The samples were mounted on a metal stub with carbon paint. The samples were thinly coated with palladium-gold under vacuum to make the surface conducting for viewing through SEM. The mounted specimens were studied by SEM (JEOL-JSM 6480 LV).

3.4.3 Phase Analysis

Phase analysis and crystallite size determination of the sintered specimen was done by XRD technique. The fundamentals and experimental method have been discussed in section 3.2.

3.4.4 Dielectric Characterization

Sintered pellet samples were taken for dielectric measurement. Firstly the samples were thoroughly cleaned by immersing them inside acetone solution taken in a small beaker and keeping that beaker in an ultrasonic bath for 15 min. Then the samples were allowed to dry in air atmosphere. After that a very thin coating of silver paste was applied on both side of the pellet

samples. Now the samples were cured at 600^0C for 30 min. After the curing is complete the samples were taken for dielectric measurements.

The Impedance Analyzer (Model SI 1260 Solartron) was used for characterization. The measurements were taken in the frequency range of 1 Hz to 1 MHz. From this characterization we were able to get the Relative Permittivity and tanδ of the ferrite samples. From there the AC resistivity of the samples were calculated by using the following formula,

$$\rho = \frac{1}{\omega \varepsilon_0 k' \tan\delta} \tag{3.8}$$

where, $\omega = 2\pi f$ = angular frequency
ε_0 = Permittivity of free space
k'= Relative Dielectric constant
tanδ = Dissipation or loss factor

After obtaining all the measurements the variation of permittivity vs frequency, tanδ vs frequency and AC resistivity vs frequency were plotted and analyzed.

3.4.5 Inductance and Magnetic Loss

Inductance and magnetic loss are the basic magnetic property of any ferrites. The LCR HiTESTER (Model 3532-50) HIOKI, with the maximum frequency limit of the instrument 5 MHz, was used to measure the inductance and tanδ on toroid samples, wound with low capacitive six turns (Fig. 5) enameled copper wire. The significance of this winding is that the stray capacitance (undesirable capacitance which can allow signals to leak between circuit wires) can be reduced by this special winding of the ferrite core [16].

The inductance of a ferrite core depends on the number of turns, diameter of the coils, the length of the coil, and the nature of the ferrite composition. By definition, inductance is the ratio

of the total magnetic flux linkage to the current (I) through the ferrite core. Total magnetic flux linkage is dependent on magnetic permeability (μ) of the medium (core material). This means inductance is directly proportional to permeability.

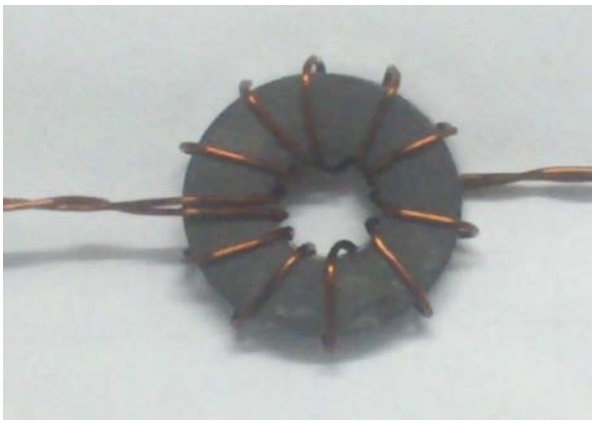

Fig. 5 Toroid sample with low capacitive six turn copper winding

Initial permeability was calculated from the inductance data as per [17] using the following formula:

$$\mu_i = \frac{L}{2*10^{-7}*Na^2*H_t*\ln[\frac{D_o}{D_{in}}]} \quad (3.9)$$

where L is the inductance, N_a is the number of turn, H_t , D_o and D_{in} are the toroid's height, outer diameter and inner diameter, respectively.

Various core losses associated with ferrites are hysteresis losses, eddy current losses and residual losses. The hysteresis loss is mainly caused by the irreversible rotation of magnetization vector. The eddy current loss is due to the current induced in the core under the influence of a time varying magnetic flux. The residual loss is generated by the power dissipation resulting

from the reversible domain wall damping and the reversible rotation of domains. The relative loss factor (RLF), i.e. the ratio of the loss tangent (tanδ) to initial permeability was calculated from tanδ and initial permeability.

Finally the variation of permeability with frequency and variation of Relative Loss Factor (RLF) with frequency were plotted and analyzed.

3.4.6 Magnetization

Saturation Magnetization was measured for the ferrite samples. The MAGNETA Pulse Field Hysteresis Loop Tracer instrument was used for the M-H loop tracing. Firstly, the instrument was calibrated using standard Nickel specimen with known magnetization. Then the pellet sample was placed inside the sample holder and a magnetic field was applied and measurements were taken. Finally the M-H loop was plotted and saturation magnetization (M_s) and coercivity field was measured.

All electrical and magnetic characterizations are within the experimental error.

CHAPTER IV

RESULTS AND DISCUSSIONS

4.1 Densification Analysis

The variations in Bulk density of sintered specimen are shown in Fig. 6. It is observed that density increases with increase in sintering temperature. At 900^0C and 950^0C the bulk density of Mg-La substituted samples are higher than other two compositions. However at 1000^0C the bulk density of Mg -La substituted samples decreases and remains at an intermediate value in between the bulk density of Mg substituted ferrite and La substituted ferrite samples.

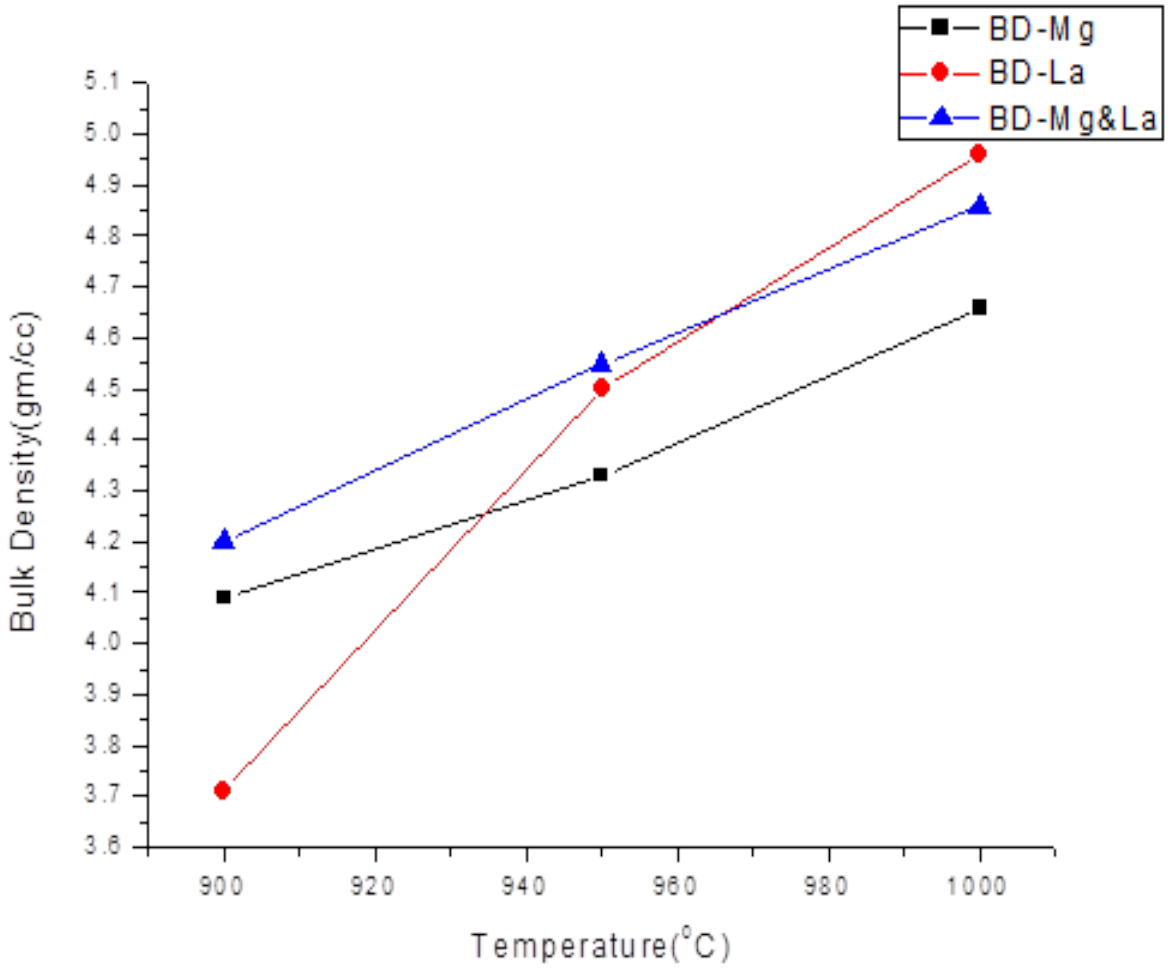

Fig 6 Variation of Bulk Density of Sintered samples with sintering temperature

4.2 Phase Analysis

The Fig. 6 shows XRD pattern of [$Ni_{0.25-0.18}$ $Mg_{0.18}$ $Cu_{0.2}$ $Zn_{0.55}$] $La_{0.025}$ $Fe_{2-0.025}O_4$ ferrite as synthesized powder. The figure shows the crystalline peaks of the ferrite. The peaks are broadened which indicate the very small crystallite size of the ferrite. The crystallite size was calculated from Full Width at Half Maxima (FWHM) of (311) peak using Scherer formula and the size was about 30nm.

The similar broaden peaks were found for Mg substituted ferrite and La substituted ferrite respectively. This indicates that the auto-combustion synthesis is very useful to synthesize nano crystalline ferrite powder at low temperature

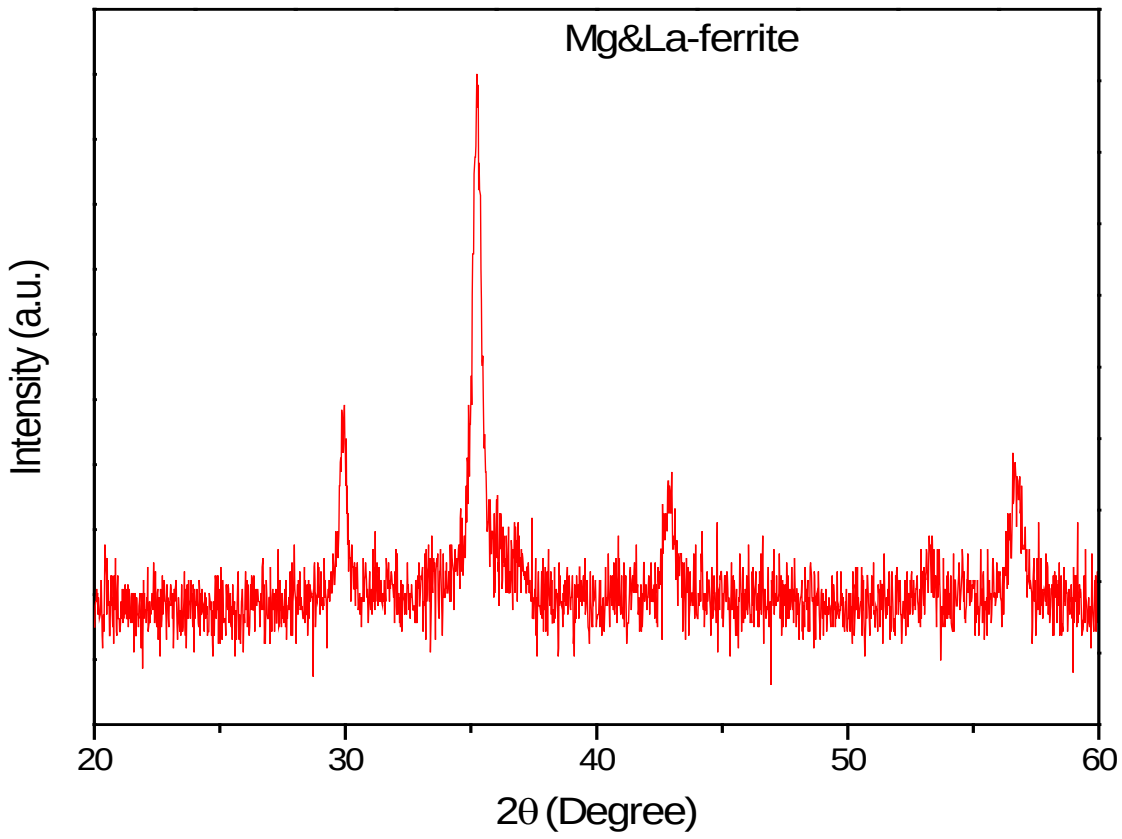

Fig. 7 XRD pattern of [$Ni_{0.25-0.18}$ $Mg_{0.18}$ $Cu_{0.2}$ $Zn_{0.55}$] $La_{0.025}$ $Fe_{2-0.025}O_4$ ferrite as synthesized powder

The as synthesized powders of all the ferrites were calcined at 700^0C for 2 hrs to get better crystallinity and homogeneous spinel phases. The Fig. 7 shows the XRD pattern of all calcined ferrites powders. The crystallite sizes of the calcined ferrites were in the range of 40-50 nm. The ferrites were sintered at 3 different temperatures: 900, 950 and 1000^0C respectively for 4 h to investigate the effect of sintering temperature on the properties of the ferrite.

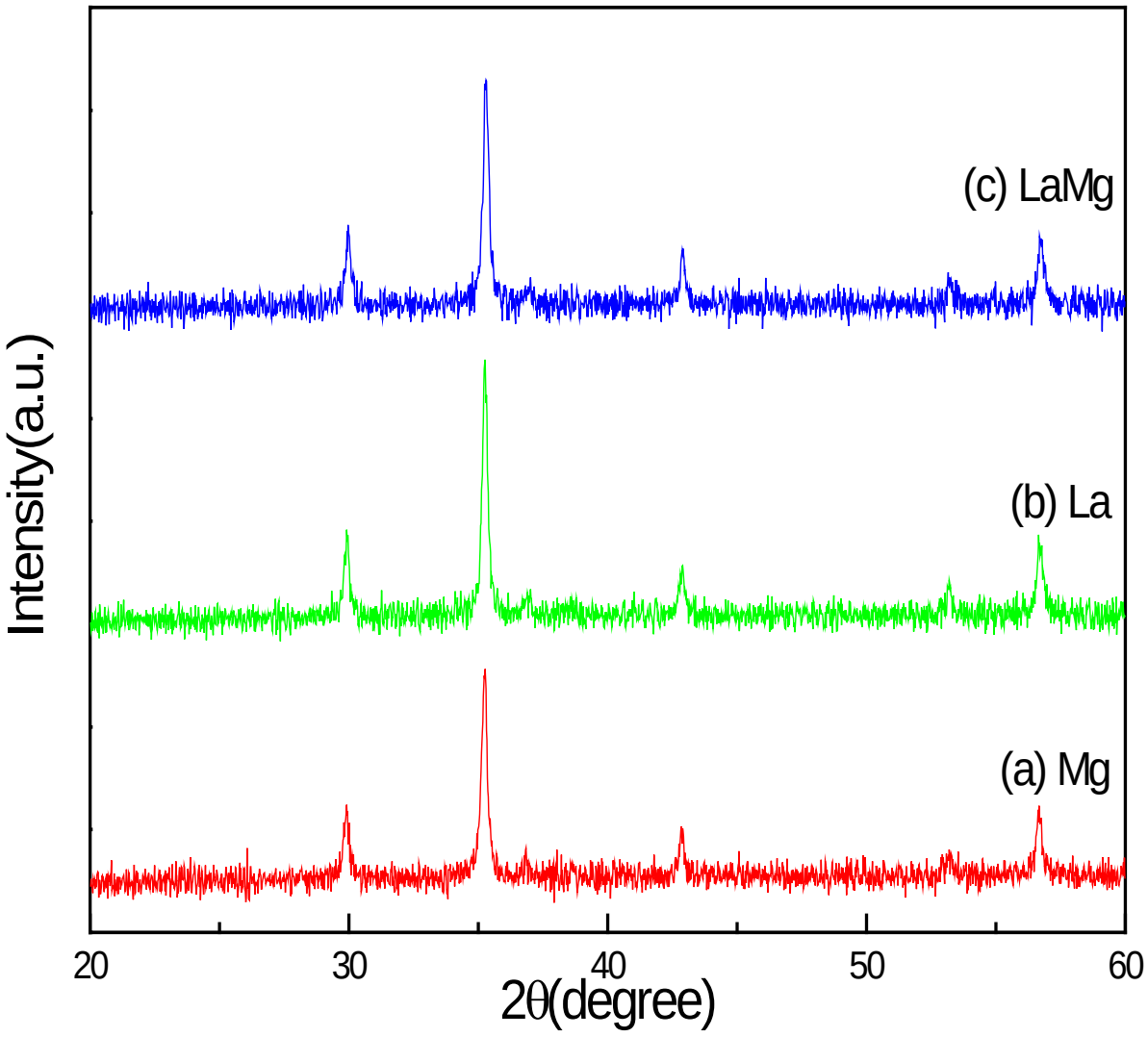

Fig. 8 XRD Pattern of NiCuZn ferrite powders calcined at 700^0C/2hrs (a) Mg substituted ferrite (b) La substituted ferrite (c) Mg&La substituted ferrite

The Fig. 8 shows that the peaks were sharp compared to as synthesized powders indicating increase in crystallite size in sintered product. The figure also shows that the diffraction peaks were shifted towards higher 2 theta with increase in sintering temperature. The lattice parameter for 3 sintered specimen were evaluated using (311) peak and they were a= 8.39 A^0 for 900^0C, a= 8.41 A^0 for 950^0C, a= 8.42 A^0 for 1000^0C sintered pellets respectively. Lattice parameter shows that it increases with increasing sintering temperature. This may be due to the more homogeneous phase formation and complete solid solution formation with increase in sintering temperature.

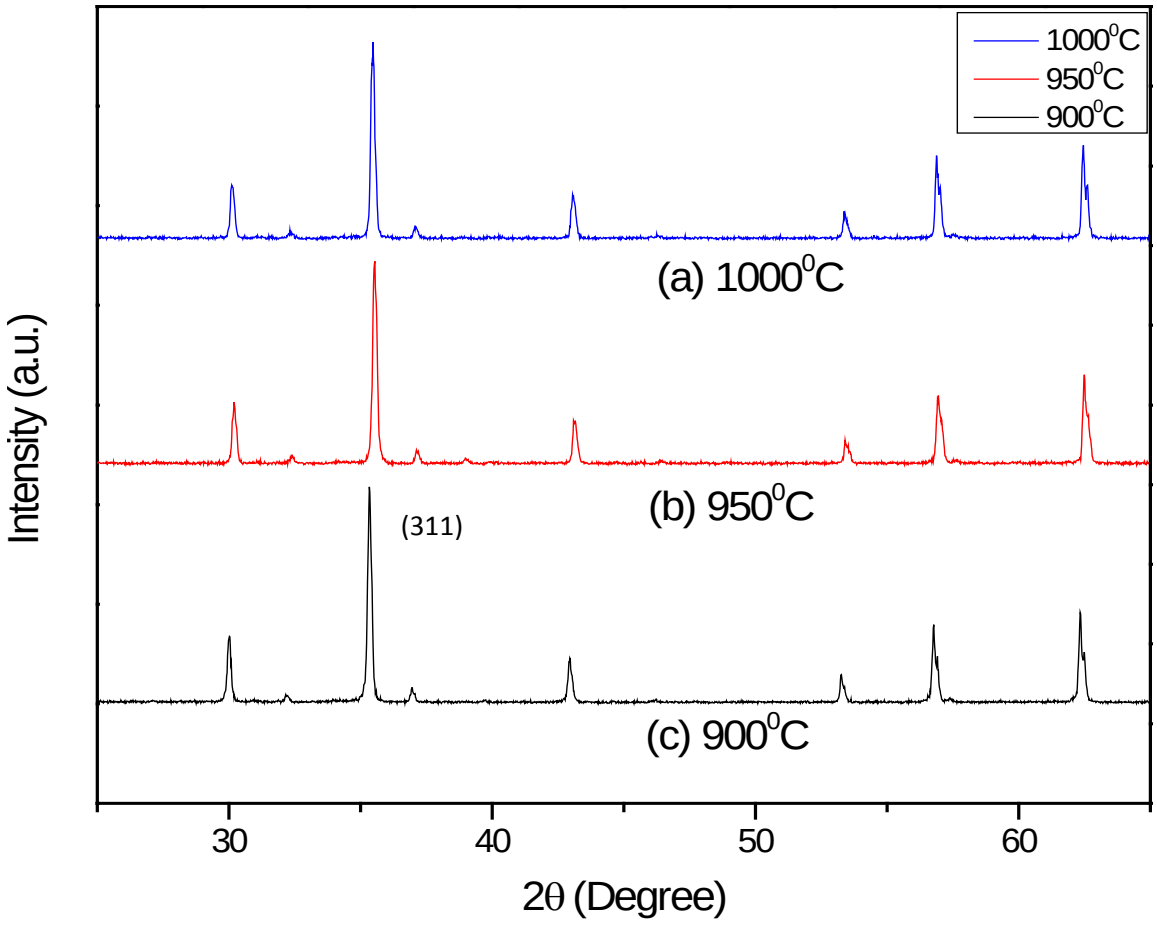

Fig. 9 XRD patterns of [$Ni_{0.25-0.18}$ $Mg_{0.18}$ $Cu_{0.2}$ $Zn_{0.55}$] $La_{0.025}$ $Fe_{2-0.025}O_4$ ferrite powder (a) sintered at 900^0C (b) sintered at 950^0C (c) sintered at 1000^0C

4.3 Microstructural Properties:

The sintered pellets were characterized for its bulk density by Archimedes principle. The bulk densities were 4.20 gm/cc, 4.46 gm/cc and 4.79 gm/cc for pellets sintered at 900^0C, 950^0C, 1000^0C respectively. The % theoretical density were calculated using XRD density of the sintered material and they were 91%, 92% and 94% respectively with increasing temperature order.

The sintered pellets were characterized for their microstructural development. Fig. 9 shows the SEM micrograph of $[Ni_{0.25-0.18}\ Mg_{0.18}\ Cu_{0.2}\ Zn_{0.55}]\ La_{0.025}\ Fe_{2-0.025}O_4$ ferrite sintered at 1000^0C. The specimen shows a uniform grain distribution with an avg. grain size of 1 micron.

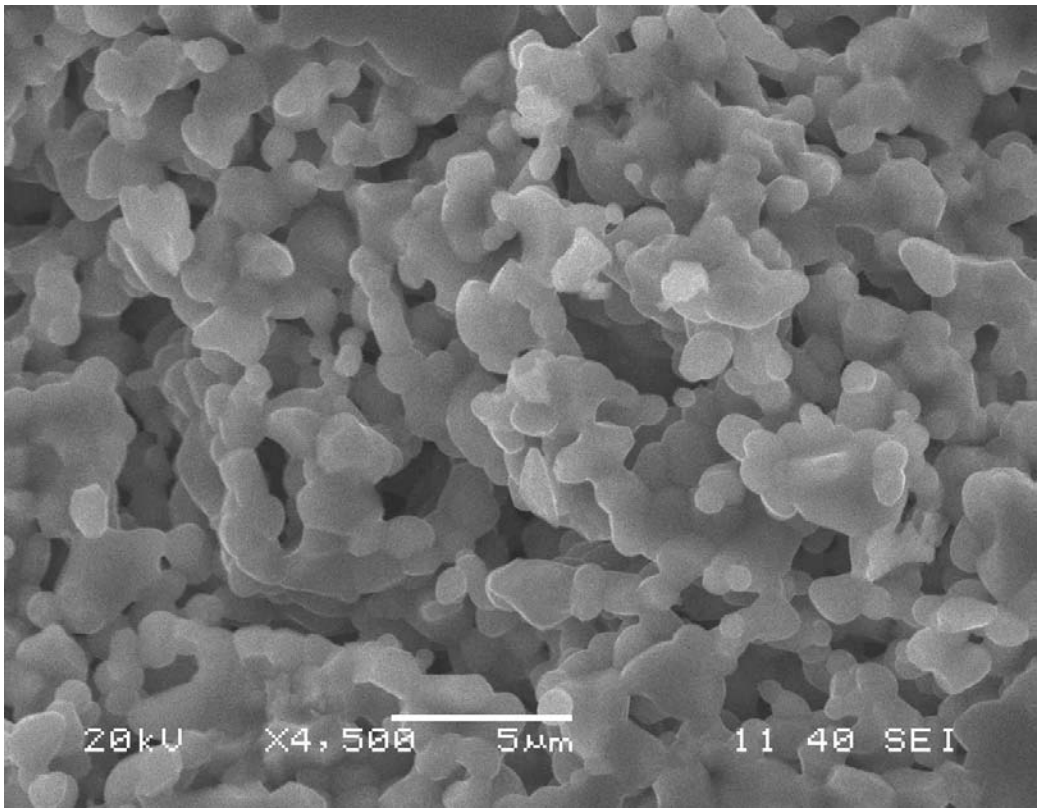

Fig. 10 SEM micrograph of $[Ni_{0.25-0.18}\ Mg_{0.18}\ Cu_{0.2}\ Zn_{0.55}]\ La_{0.025}\ Fe_{2-0.025}O_4$ ferrite sintered at 1000^0C.

4.4 Electromagnetic Properties:

Electromagnetic properties of different ferrites were measured on toroid specimen. The variation of permeability with measuring frequency is shown in Fig. 10. The Figure shows that the permeability of Mg & La substituted ferrite is higher than La substituted ferrite. However this is lower than the Mg substituted ferrite. All the composition shows a stable permeability up to about 1 MHz. Above that frequency the permeability dispersion occurs in all the ferrites.

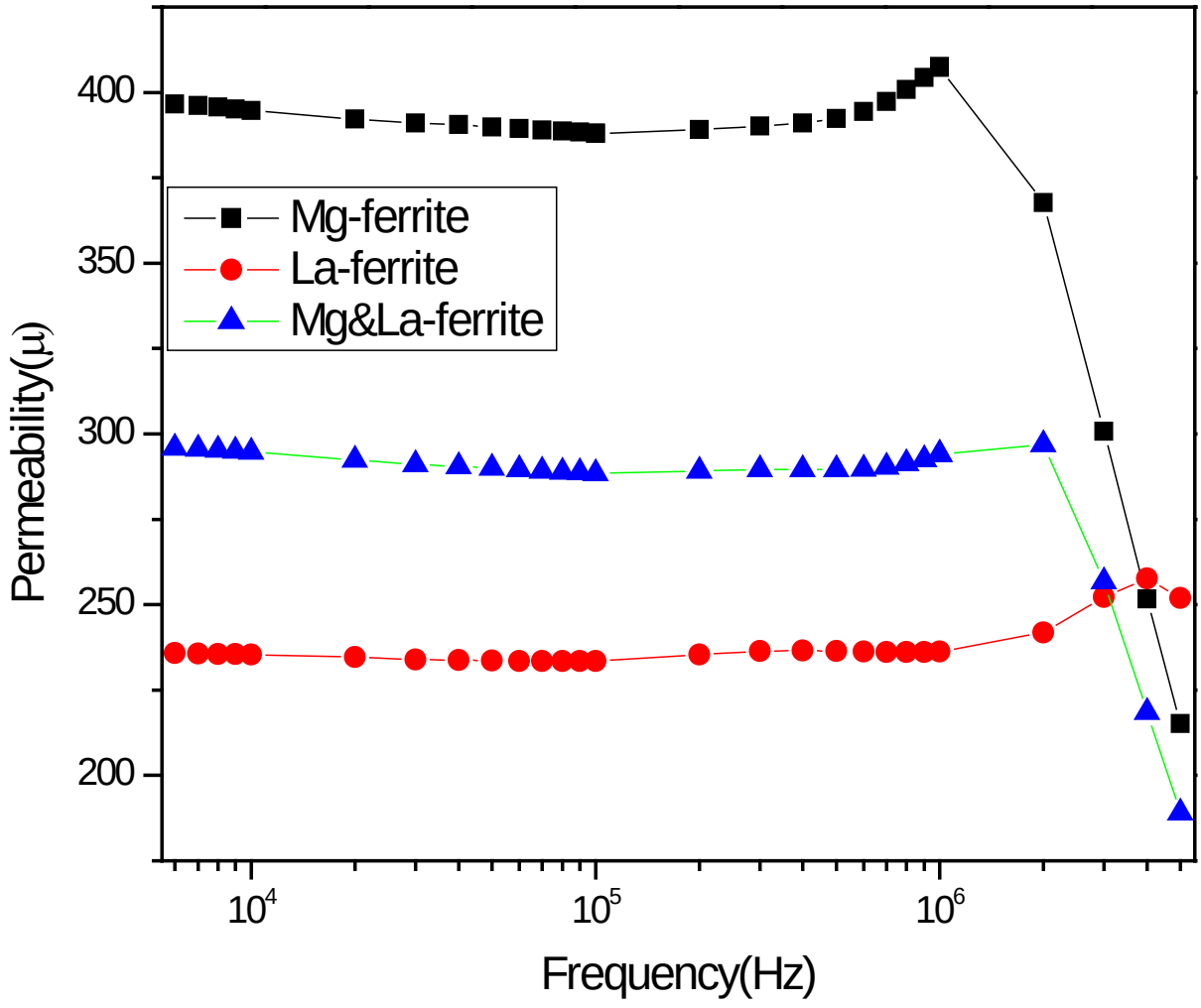

Fig. 11 Frequency dependency of initial permeability in 3 compositions of ferrites sintered at 1000^0C

The permeability peak frequency i.e. the cut off frequency was found to increase in the order Mg substituted ferrite to Mg & La substituted ferrite to La substituted ferrite. The dispersion is due to the domain wall dynamics as explained by [18]. We know that cut off frequency is inversely proportional to the magnetic permeability as per Snoek's law [19]. That is why the Mg substituted ferrite has the lowest cutoff frequency due to its highest permeability among all 3 compositions. So these results conclude that the permeability of La substituted NiCuZn ferrite can be enhanced by the substitution of 'Mg' for 'Ni' in the ferrite.

To investigate the effect of sintering temperature on the permeability of Mg & La substituted NiCuZn ferrite the permeability of different sintered specimen were plotted with frequencies (Fig. 11).

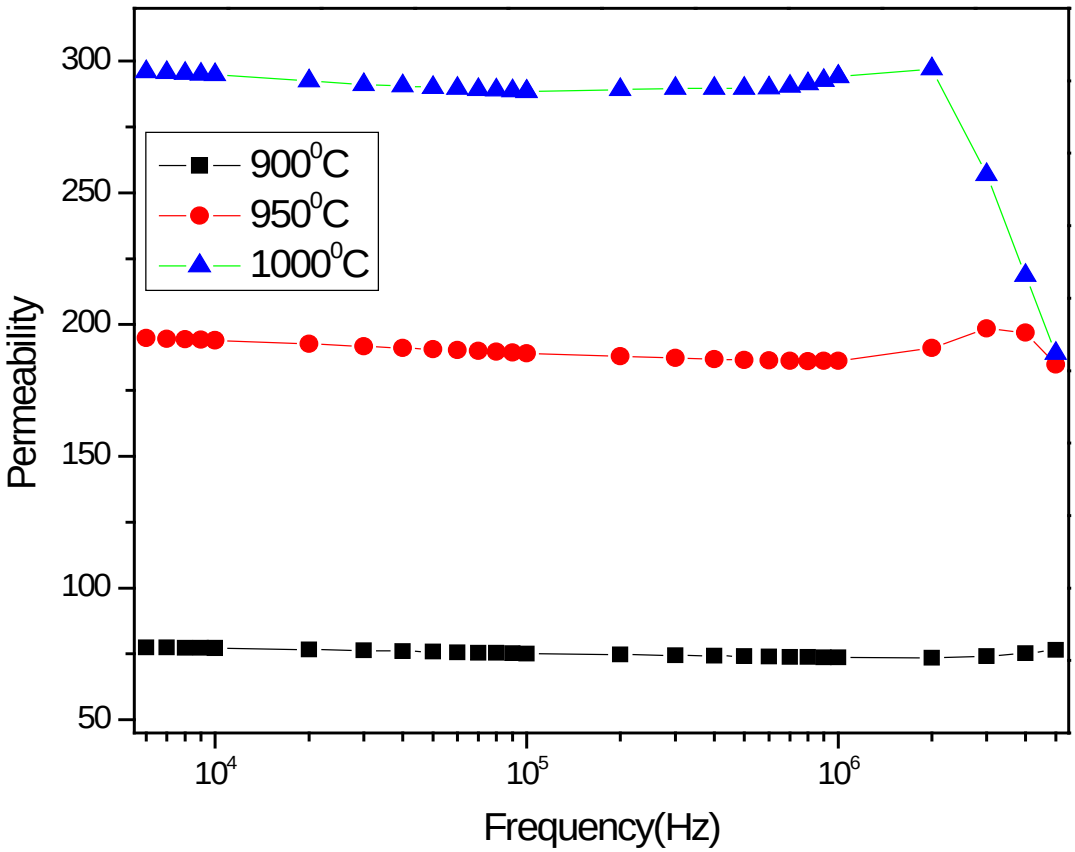

Fig. 12 Frequency dependency of initial permeability in Mg & La substituted ferrite sample sintered at 900^{0}C, 950^{0}C, 1000^{0}C

The Fig. 11 indicates that the permeability increase with increase in sintering temperature from 75 to 300 with the increase of 1000C in sintering temperature. This is due to the increase in Bulk Density/ grain size with sintering temperature. We know that Magnetization increases with increase in density of ferrite [20]:

$$M = D_{Bulk} * \sigma \quad (3.10)$$

And the initial permeability increases with grain size as per Globes Model [20]:

$$\mu = \frac{3\, l_0 M_s^2 D}{16 \gamma w} \quad (3.11)$$

The initial permeability increases linearly with grain size/ Bulk Density.

The Relative Loss Factor (RLF) is the ratio of magnetic loss tangent (tan δ) to initial permeability (μ). For high frequency inductor core application a high μ and low RLF is required. The Fig. 12 shows that the RLF of Mg & La substituted NiCuZn ferrite decreases with increasing in sintering temperature due to the decrease in porosity and increase in domain size. RLF also decreases with increase in frequency as we know that the tan δ is inversely proportional to the frequency. However the RLF again increases above 1 MHz. This may be due relaxation losses in the ferrite as they are in the cutoff frequency zone stated above.

The magnetic relaxation is considered to be the reason for delay in domain wall motion with respect to change in externally applied magnetic field.

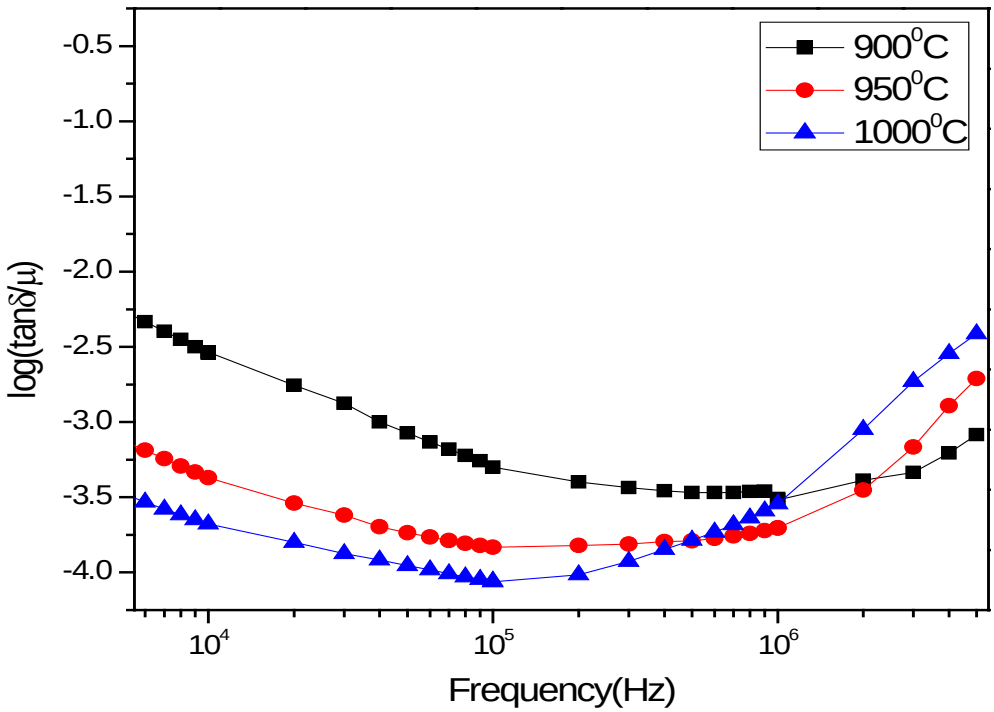

Fig. 13 Relative loss factor as a function of frequency for Mg & La substituted NiCuZn ferrite sintered at different temperature

4.5 Dielectric Properties

The Fig. 13 shows the variation of relative permittivity with frequency. The Permittivities were stable in the frequency range 10^3 to 10^6 Hz and it was relatively small for all the three ferrites. The Fig. 14 shows the variation of tan δ with frequency for the ferrites. It shows that the loss of La substituted NiCuZn ferrite is higher than other ferrites in the MHz range whereas in the KHz range the loss is highest in Mg substituted NiCuZn ferrite. Mg & La substituted NiCuZn ferrite loss in between these two. These relative permittivity and loss factor is very important for Multi-Layer Chip Inductor (MLCI). Where ferrite thin films are separated by electrodes and the parasitic capacitance of this assembly is very important for multilayer devices. The capacitance and tan δ should be as low as possible for a good inductor material. All the ferrite shows very low capacitance and loss factor (tan δ).

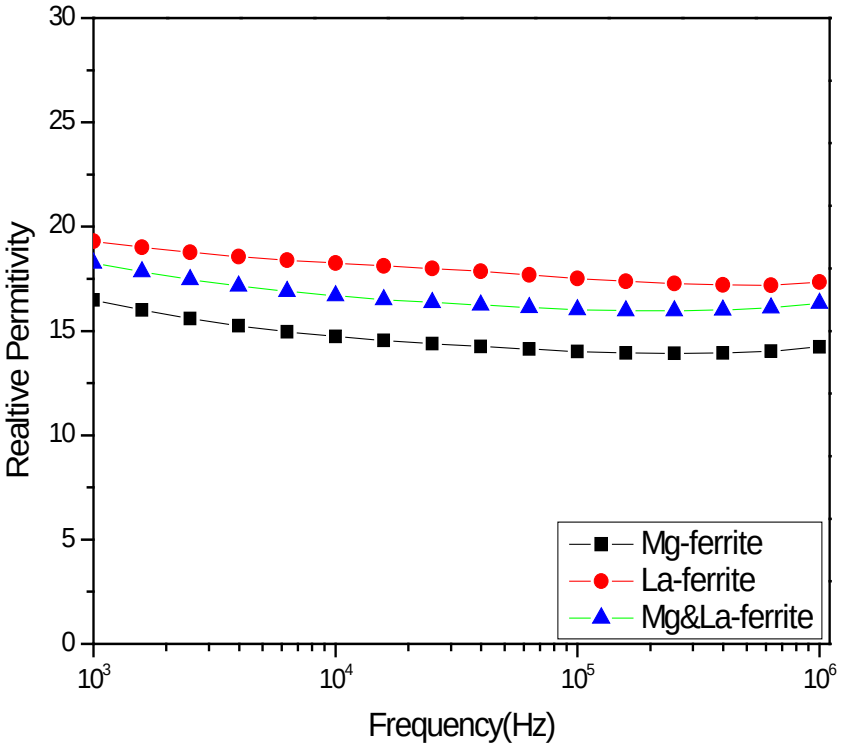

Fig. 14 Frequency dependency of Relative permittivity of 3 different ferrite compositions sintered at 1000^0C

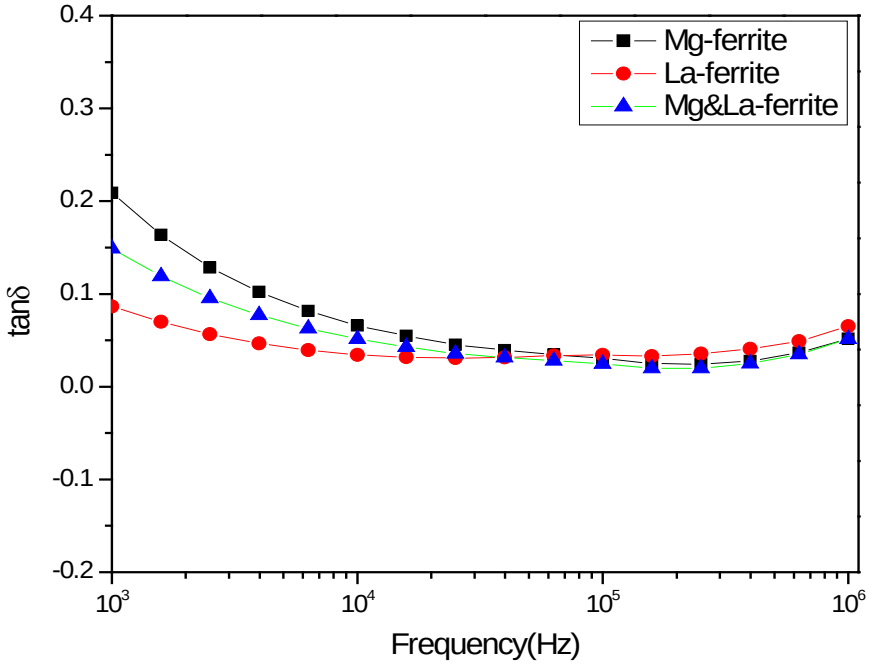

Fig. 15 Frequency dependency of Loss Factor of 3 different ferrite compositions sintered at 1000^0C

The AC Resistivity is also an important characteristic of these ferrites in multilayer structures. Fig. 15 shows the variation of AC resistivity of the ferrites with frequency.

The figure indicates that Mg & La substituted NiCuZn ferrite has higher AC resistivity in higher frequency zone. All these results conclude that Mg & La substituted NiCuZn ferrite could be a good core material for inductor in MHz application area.

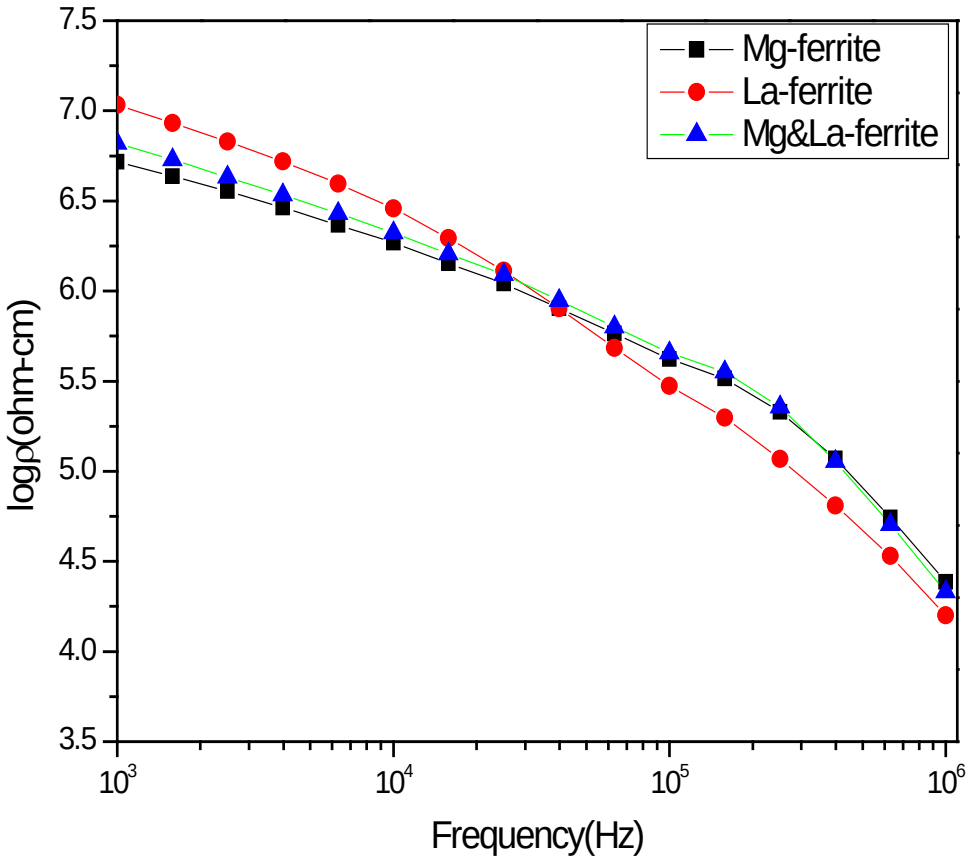

Fig. 16 AC resistivity as a function of frequency in all the 3 different compositions of NiCuZn ferrite samples sintered at 1000^0C

4.6 Magnetization

The Fig. 16 shows the hysteresis curve of the ferrite compositions sintered at 1000^0C. The saturation magnetization was highest for La substituted NiCuZn ferrite. However the magnetization of Mg substituted NiCuZn ferrite was increased by the La substitution in it. The magnetic hysteresis loop shows that the materials have low hysteresis loss with high permeability depicting the typical soft ferrite characteristics.

Magnetization study also shows that La substitution in Mg substituted NiCuZn ferrite may be a good material for high frequency inductor core applications.

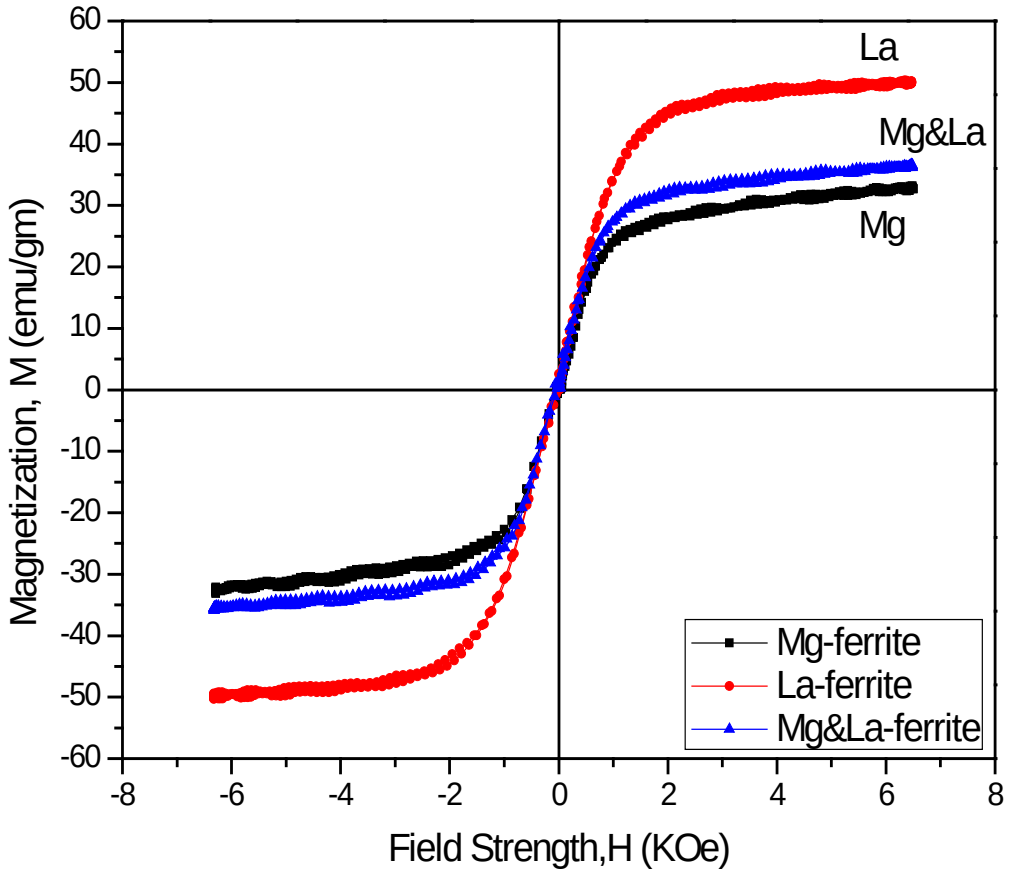

Fig. 17 Magnetic hysteresis curve for 3 different compositions of NiCuZn ferrite samples sintered at 1000^0C

CHAPTER V

CONCLUSION

CONCLUSION:

The effect of La and Mg substitution on NiCuZn ferrite has been investigated. The complex ferrite composition was successfully synthesized through sol-gel auto-combustion process. The ferrites were sintered in the temperature range 900^0C to 1000^0C. In general, the initial permeability of all the ferrite increased with increase in sintering temperature due to the increased densification and grain size. The initial permeability of La substituted NiCuZn ferrite substantially improved by Mg substitution in the ferrite. This may be due to better densification and lowering of magnetostriction by the substitution . Also the substitution enhances the resistivity of the ferrite. So, the Mg substituted La-NiCuZn ferrite would be a better material for multilayer chip inductor core material useable in high frequency application.

CHAPTER VI

REFERENCES

REFERENCES

[1] US patent no. 2011/0226982 A1

[2] J. H. Jean, C. H. Lee, W. S. Kou, J. Am. Ceram. Soc. 82 (2) (1999) 343.

[3] J. Z. Msomi, T. Moyo, T. B. Doyle, J. Magn. Magn. Mater. 310 (2007) 2534.

[4] O. F. Caltun, L. Spinu, Al. Stancu, L. D. Thung, W. Zhou, J. Magn. Magn. Mater. 242–245 (2002) 160.

[5] J. Y. Hsu, W. S. Ko, H. D. Hen, C. J. Chen, IEEE Trans. Mag. 30 (6) (1994) 4875.

[6] Ailin Xia n, ChuanguiJin,DexinDu,GuohuiZhu Journal ofMagnetismandMagneticMaterials323(2011)1682–1685

[7] Jin Woo Hahn, Kang Ryong Choi Thin Solid Films 519 (2011) 8388–8390

[8] P. Guzdek , J.Kulawik,K.Zaraska,A.Bien´ kowski Journal ofMagnetismandMagneticMaterials322(2010)2897–2901

[9] Hua Su, Huaiwu Zhang, Xiaoli Tang, Yulan Jing, and Baoyuan Liu IEEE TRANSACTIONS ON MAGNETICS, VOL. 45, NO. 5, MAY 2009

[10] K.H. Rao Structural and magnetic properties of Mg substituted NiCuZn Nano Ferrites

[11] P.K. Roy, J. Bera Effect of Mg substitution on electromagnetic properties of $(Ni_{0.25}Cu_{0.20}Zn_{0.55})Fe_2O_4$ Ferrite prepared by auto combustion method

[12] P.K. Roy, J. Bera Effect of La substitution on electromagnetic properties of NiCuZn Ferrite prepared by auto combustion method

[13] T. Nakamura, J. Magn. Magn. Mater. 168 (1997) 285.

[14] H. I. Hsiang, W. C. Liao, Y. J. Wang, Y. F. Cheng, J. Magn. Magn. Mater. 24 (7) (2004) 2015.

[15] K. O. Low, F. R. Sale, J. Magn. Magn. Mater. 246 (2002) 30.

[16] J. Smit, H. P. J. Wijn, Ferites, John Wiley & Sons, New York (1959).

[17] Z. Yue, L. Li, J. Zhou, H. Zhang, Z. Gui, Mat. Sci. Engg. B 64 (1999) 68.

[18] M. D. Nersesyan, A. G. Peresada, A. G. Merzhanov, Int. J. SHS 7 (1998) 60.

[19] S. R. Jain, K. C. Adiga, Combustion and Flame 40 (1981) 71.

[20] Y. Bai, J. Shou, Z. Gui, Z. Yue, L. Li, J. Magn. Magn. Mater. 264 (2003) 44.